Dalton Transactions

Accepted Manuscript

This is an *Accepted Manuscript*, which has been through the Royal Society of Chemistry peer review process and has been accepted for publication.

Accepted Manuscripts are published online shortly after acceptance, before technical editing, formatting and proof reading. Using this free service, authors can make their results available to the community, in citable form, before we publish the edited article. We will replace this *Accepted Manuscript* with the edited and formatted *Advance Article* as soon as it is available.

You can find more information about *Accepted Manuscripts* in the Information for Authors.

Please note that technical editing may introduce minor changes to the text and/or graphics, which may alter content. The journal's standard Terms & Conditions and the Ethical guidelines still apply. In no event shall the Royal Society of Chemistry be held responsible for any errors or omissions in this *Accepted Manuscript* or any consequences arising from the use of any information it contains.

ROYAL SOCIETY OF CHEMISTRY

www.rsc.org/dalton

Molecular Layer Deposition of "titanicone", a titanium-based hybrid material, as an electrode for lithium-ion batteries

Kevin Van de Kerckhove,[*,†] Felix Mattelaer,[†] Davy Deduytsche,[†] Philippe M. Vereecken,[‡,¶] Jolien Dendooven,[†] and Christophe Detavernier[†]

Department of Solid State Sciences, Ghent University, Krijgslaan 281 S1, 9000 Gent, Belgium, imec, Kapeldreef 75, 3001 Leuven, Belgium, and Centre for surface chemistry and catalysis, KU-Leuven, 3001 Leuven, Belgium

E-mail: kevin.vandekerckhove@ugent.be

Dalton Transactions Accepted Manuscript

Abstract

Molecular layer deposition (MLD) of hybrid organic-inorganic thin films called "titanicones" was achieved using tetrakisdimethylaminotitanium (TDMAT) and glycerol (GL) or ethylene glycol (EG) as precursors. For EG, in situ ellipsometry revealed that film growth initiates, but terminates after only 5 to 10 cycles, probably because both hydroxyls react with the surface. GL has a third hydroxyl group, and in that case steady state growth could be achieved. The GL process displayed self-limiting reactions for both reactants in the temperature range from 80 °C to 160 °C, with growth rates of 0.9 to 0.2 Å /cycle, respectively. Infrared (FTIR) and X-ray photoelectron spectroscopy (XPS) confirmed the hybrid nature of the films,

[*]To whom correspondence should be addressed
[†]Ghent University
[‡]imec
[¶]CSCC

with a carbon atomic concentration of about 20%. From X-ray reflectivity, the density was estimated at 2.2 g/cm^3. A series of films was subjected to water etching and annealing in air or He atmospheres at 500 °C. The carbon content of the films was monitored with FTIR and XPS. Almost all carbon was removed from the air annealed and water treated films. The He annealed samples however retained their carbon content. Ellipsometric porosimetry (EP) showed 20% porosity in the water etched samples, but no porosity in the annealed samples. Electrochemical measurements revealed lithium ion activity during cyclic voltammetry in all treated films, while the as-deposited film was inactive. With increasing charge current, the He annealed samples outperformed amorphous and anatase TiO_2 references in terms of capacity retention.

Introduction

Molecular layer deposition (MLD) is a thin film deposition technique where hybrid organic-inorganic films are grown by exposing the substrate to subsequent, self-limiting, (metal-)organic precursor gases. The method is very closely related to atomic layer deposition (ALD) of inorganic layers.[1] Therefore it exhibits many of the attractive properties of ALD, such as precise thickness control and conformality on high aspect ratio structures. MLD is known in literature since the early 90's for the deposition of polymer films.[2] Only more recently, interest in hybrid organic-inorganic thin films has arisen.[3] These hybrid films display several intriguing properties and applications in flexible electronics and photo-catalysis.[4–6] Today, several MLD processes have already been developed for various hybrid materials, called 'metalcones', by combining known metal-organic precursors from ALD with organic reactants as ethylene glycol (EG) and glycerol (GL). The alucone process for an aluminium oxide hybrid is the most extensively studied and many processes using different organic compounds exist.[3,7–9] Other metalcones known in literature are zincone[10,11], zircone[12], hafnicone[13] and titanicone[14–17]. It has been shown that these metalcones can be transformed into porous metal oxides through water etching and calcination in air.[18]

Dalton Transactions Accepted Manuscript

Table 1: Overview of known titanicone processes in literature.

	EG[15]	GL[15]	4-Aminophenol[16]	4,4'-oxydianiline[17]
Growth rate per cycle (Å)	4.3	2.6	11	0.7
Temperature window (°C)	80-135	130-210	120-160	250-490
Density (g/cm^3)	1.8	1.8	1.9-2.2	/
Stable in air?	No	Yes	Yes	Yes

Titanicones have received much attention in the last years. A short overview of titanicone processes known in literature up to now is presented in table 1. All these processes are based on $TiCl_4$ as the titanium precursor. $TiCl_4$ is a relatively small molecule, and combined with the larger organic reactants it leads to high growth rates which are mainly limited by steric hindrance caused by the organic reactants. It has been reported that these titanicones can be transformed into conductive films through pyrolysis at temperatures up to 900 °C[19]. Since ALD TiO_2 is a known anode material for lithium-ion batteries[20], there could be heat or other treatments to be discovered that activate the film as a working electrode material.

In this work, tetrakis(dimethylamino)-titanium (TDMAT) has been investigated as an alternative titanium precursor for $TiCl_4$. TDMAT is a well-known precursor in ALD literature and is suited for the deposition of TiO_2 and TiN by both thermal and plasma enhanced processes[21–23]. Here, TDMAT has been combined with both EG and GL as organic reactants. With the application of in situ ellipsometry measurements, the process parameters could be optimized. Ex situ techniques enabled the study of the titanicone film characteristics, such as morphology and composition. A series of films were subjected to several post-deposition treatments, such as water etching and annealing in air and He atmospheres. The influence of these treatments on film properties was investigated. Additionally, the films were tested for lithium-ion electrochemical activity and compared to amorphous and anatase TiO_2 reference samples.

Dalton Transactions Accepted Manuscript

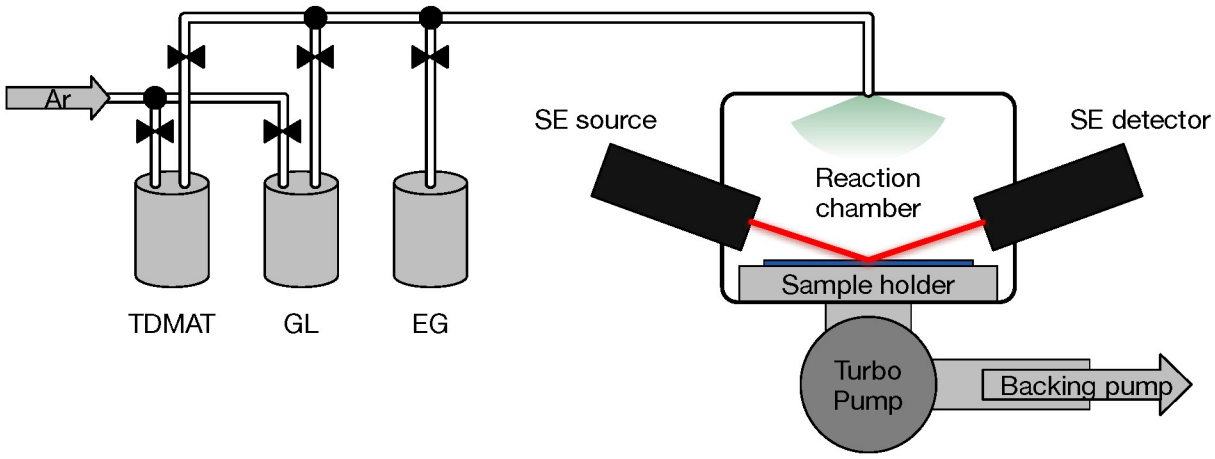

Figure 1: A simplified schematic diagram of the molecular layer deposition reactor.

Experimental

For the deposition of the hybrid titanicone films, a dedicated reaction chamber was designed and constructed out of stainless steel. A schematic representation of the system can be seen in Figure 1. The reaction chamber was continuously pumped down by a turbo-molecular pump to a base pressure in the range of 10^{-6} mbar. The deposition chamber was heated to a temperature of 120 °C to avoid condensation of the organic reactants. The samples were heated by a copper block fitted with resistive cartridge heaters. The sample temperature was continuously monitored and regulated precisely by a PID controller with an attached thermocouple. The bubbler containing the TDMAT precursor (99.999%, Sigma-Aldrich) was kept at a constant temperature of 30 °C for stability. The TDMAT delivery line was heated to 50 °C. The precursor was dosed into the reaction chamber in an argon (99.999% pure, Air Liquide) flow, due to its low vapor pressure. The EG container (99.997%, Sigma-Aldrich) was heated to 80 °C and required no carrier gas. The GL precursor (99.5%, Sigma-Aldrich) remained at a constant temperature of 60 °C and was pulsed into the deposition chamber in an argon flow. The standard substrate for process development was Si with 100 nm thermal oxide on top. For the electrochemical measurements a Si substrate with an 80 nm Pt current collector on top of 60 nm TiN was employed, both deposited by physical vapor deposition (PVD).

On this homebuilt MLD reactor a spectroscopic ellipsometer (SE) could be attached, enabling in

Dalton Transactions Accepted Manuscript

situ monitoring of the optical properties of the film during the process. The ellipsometer (J.A. Woollam, Model M-2000) operates in the ultraviolet to near infrared region. The data was analyzed in the provided CompleteEASE software package. The optical model consisted of a fixed Si substrate and 100 nm SiO_2 layer, with the titanicone layer, modelled by a Cauchy dispersion relation with the thickness as the only adjustable parameter, on top. The optical parameters of the titanicone layer were calibrated through several samples for which the thickness was determined by X-ray reflectivity (XRR) measurements.

X-ray diffraction (XRD), X-ray fluorescence (XRF) and XRR measurements were performed on a Bruker D8 Discover diffractometer. XRD and XRR employed a Cu Kα X-ray source ($\lambda = 0.154$ nm). For XRF, a Mo Kα source was used ($\lambda = 0.071$ nm) on an Artax system from Bruker with an XFlash 5010 silicon drift detector. In situ XRD data during annealing was carried out on a homebuilt setup fitted with a position-sensitive detector under helium and ambient atmospheres. X-ray photoelectron spectroscopy (XPS) was performed using Al Kα radiation ($\lambda = 0.834$ nm) on a Thermo Scientific Theta Probe system. After measurement, the resulting spectra were analyzed with the CasaXPS software package for calculation of atomic concentrations.

Scanning electron microscopy (SEM) images, along with energy-dispersive X-ray spectroscopy (EDX) measurements, were acquired on a Quanta 200F (FEI) SEM instrument using a 10 keV electron beam. Together with SEM imaging, atomic force microscopy (AFM) was utilized to study the morphology of the films. The rms roughnesses were fitted from 1 μm^2 sized images, gathered by a Bruker Dimension Edge microscope.

Ellipsometric porosimetry (EP)[24,25] was used to determine the porosity, pore size distribution (PSD) and shape of porous films. In this setup, the change in refractive index is measured while filling the pores with toluene vapor. After evacuation of the system, this vapor is dosed into the chamber by a controllable valve. This valve allows to gradually increase the pressure in the chamber while simultaneously taking ellipsometry measurements. From the SE data, the adsorption and desorption isotherms can be derived, and information on the porosity, PSD and pore shapes can be attained. Prior to measurement, all samples were dried in a tube furnace for at least 4 hours at

Dalton Transactions Accepted Manuscript

100 °C to remove any condensed water from the pores. A Vertex 70v Fourier-transform infrared (FTIR) spectrometer from Bruker was employed for infrared spectroscopy. Internally, a globar source (mid IR), KBr beamsplitter and DLaTGS detector were installed on the optics bench. Electrochemical measurements were performed with a Metrohm Autolab PGSTAT302 potentiostat, connected to a three-electrode setup, inside an argon-filled glove box (O_2 and H_2O content below 1 ppm). Contacting of the Pt current collector to copper foil was done with silver paste on the edges of the sample. A solution of 1M $LiClO_4$ in propylene carbonate (99%, io-li-tec) functioned as the Li^+ electrolyte. The counter and reference electrodes for the measurements were pure lithium strips (99.9%, Sigma Aldrich). Cyclic voltammetry (CV) measurements were performed between the boundaries of 0.8 to 3.2 V at a sweep rate of 10 mV/s. Galvanostatic charging and discharging experiments were executed at currents ranging from 1 µA to 10 mA. The area of the cell was 0.9503 cm^2.

Results and discussion

Titanicone MLD with the TDMAT precursor

Firstly, we will discuss two MLD processes based on the TDMAT precursor: the EG and the GL process. EG is the most well-known organic reactant in MLD literature and thus was a straightforward choice for the development of a new process. With the help of in situ SE, the film thickness could be measured after every cycle. The TDMAT/EG process sequence is as follows: 60 s TDMAT, 60 s pump time, 45 s EG, 60 s pump time. The pressure of the TDMAT precursor with the argon flow was set to 5×10^{-3} mbar; the pressure of the EG precursor was held at 2×10^{-2} mbar. As seen in figure 2a, initial film growth is observed during the first 5 cycles. Then, the growth per cycle (GPC) rapidly decreases to less than 0.1 Å per cycle. It appears that active surface sites are being removed in the first cycles of the process, thus terminating the film growth. Even after executing 300 cycles, the resulting film thickness remains unmeasurable by XRR, hence below a few nanometers. For this reason, the optical model used for analyzing the ellipsometry data is

Dalton Transactions Accepted Manuscript

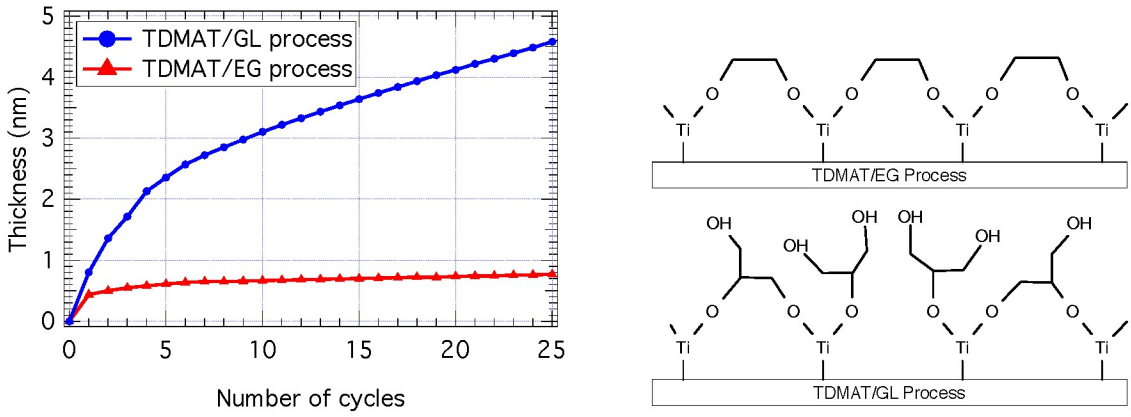

(a) (b)

Figure 2: (a) Comparison between the titanicone film growth during the first 25 cycles of the TDMAT/EG and TDMAT/GL processes, using in situ SE data. The sample temperature was 100 °C. (b) Schematic comparison of both processes, illustrating the double EG surface reactions.

based on the working TDMAT/GL process and may not be perfectly accurate for this process. The TDMAT/EG process was tested at temperatures ranging from 80 to 150°C, and EG pulse durations up to 180 s. Similar behavior as shown in figure 2a was observed at each temperature and pulse length. A possible cause of the growth termination is the previously reported effect of EG reacting twice with the surface[3]. Reactive sites are bridged by EG without offering new hydroxyl species for the TDMAT molecule. This is illustrated in figure 2b. Previous reports on this effect show a gradual decrease with increasing cycle number in contrast to the very abrupt termination here. For the working $TiCl_4$/EG process reported in literature the etching effect of HCl formed during the process may explain why this growth termination is not seen there.[17]

Next, the TDMAT and GL process was investigated. Glycerol is an organic molecule with three hydroxyl groups available for reaction. For this process it was expected for the growth termination to significantly diminish or even completely disappear. Even when two hydroxyl groups of the GL molecule react with the surface, a third group still remains available for continued growth. This is also illustrated in figure 2b. The film growth during the first 25 cycles of the TDMAT/GL process, based on in situ SE data, is shown in figure 2a, and compared with the TDMAT/EG process. The process sequence was the following: 90 s TDMAT pulse, 45 s pump time, 120 s GL pulse, and 60 s pump time. It is clear that the growth rate was significantly higher than for the EG-based process.

Dalton Transactions Accepted Manuscript

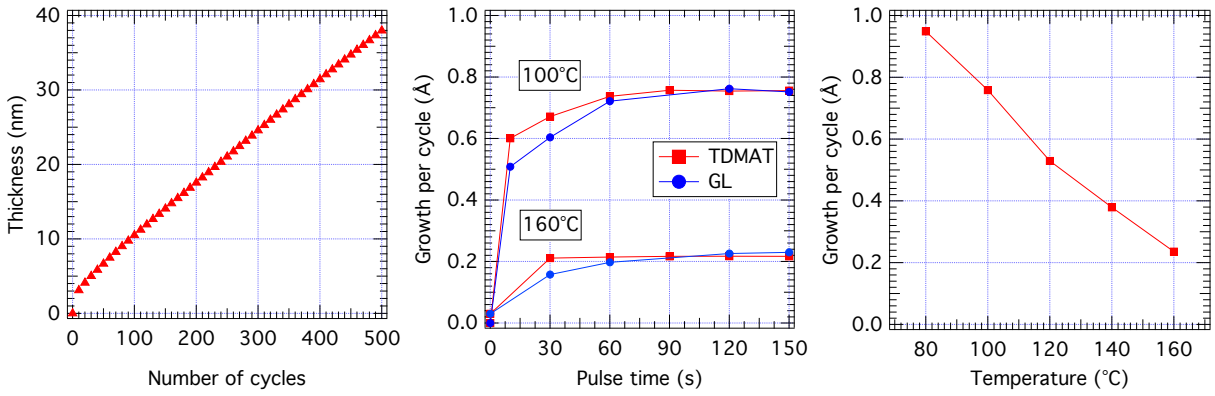

(a) (b) (c)

Figure 3: Process characteristics of the TDMAT/GL MLD, based on in situ SE data combined with ex situ XRR thickness measurements. (a) Linearity is shown for up to 500 cycles at a temperature of 100 °C. (b) Saturation curves for both TDMAT and GL precursors. (c) Temperature window where stable growth was observed. GPC decreases with increasing temperature.

Substrate-enhanced growth was observed at the start of the process. After about 10 cycles the GPC stabilized to a value of 0.76 Å/cycle at a sample temperature of 100 °C. The growth rate then remained stable for cycle numbers up to 500, thus good linearity was achieved as shown in figure 3a. The curves displayed in figure 3b show that saturation was achieved for both precursors. The GPC saturated at TDMAT pulse times higher than 90 s and GL pulse times above 120 s. Also, zero film growth was observed when dosing only TDMAT or GL into the reaction chamber. This provides clear evidence for the self-limiting nature of each surface reaction. The pulse times needed to reach saturation for this process were higher than what is usually reported in MLD literature. The reason for this is probably a combination of two effects. First, the homebuilt MLD setup is a pump-type system. In ALD literature it is generally known that these systems require higher pulse times compared to flow-type systems. Secondly, the GL was kept at a temperature of 60 °C where its vapor pressure was low. Hence, a supporting argon flow and long exposure times were necessary. The TDMAT/GL process was stable in a broad temperature window ranging from 80 °C (lowest sample temperature attainable in the hot-wall reactor) to 160 °C (limited by TDMAT decomposition). The growth rate decreased with increasing temperature, from 0.95 Å/cycle at 80 °C to 0.24 Å/cycle at 160 °C, which was also observed for TDMAT-based TiO_2 ALD processes[21–23]. In literature, this

Dalton Transactions Accepted Manuscript

was attributed to an increased TDMAT desorption from the surface at higher temperatures[21].

Characterization of the as-deposited titanicone film

The composition, morphology and other properties have been studied on as-deposited titanicone films with a thickness of 38 nm. The samples were deposited with a TDMAT/GL process of 500 cycles at a temperature of 100 °C.

The composition of the films was studied using FTIR, XPS, XRF and SEM-EDX. Both XRF and SEM-EDX data show a clear titanium signal, providing evidence for the presence of Ti in the film. Infrared spectroscopy provides more detailed information regarding the chemical bonds in the film. The spectrum gathered by FTIR is shown in figure 4. Multiple characteristic absorption modes for both carbon and titanium related groups can be observed. At wavenumbers 2928 cm^{-1} and 2870 cm^{-1}, CH_2 stretches originating from the GL molecule (TDMAT only contains methyl groups) can be found, together with a smaller absorption at 1248 cm^{-1}. The stronger C-C and C-O absorptions at 1135 cm^{-1} and 1086 cm^{-1} can also be linked to the GL molecule[3]. At low

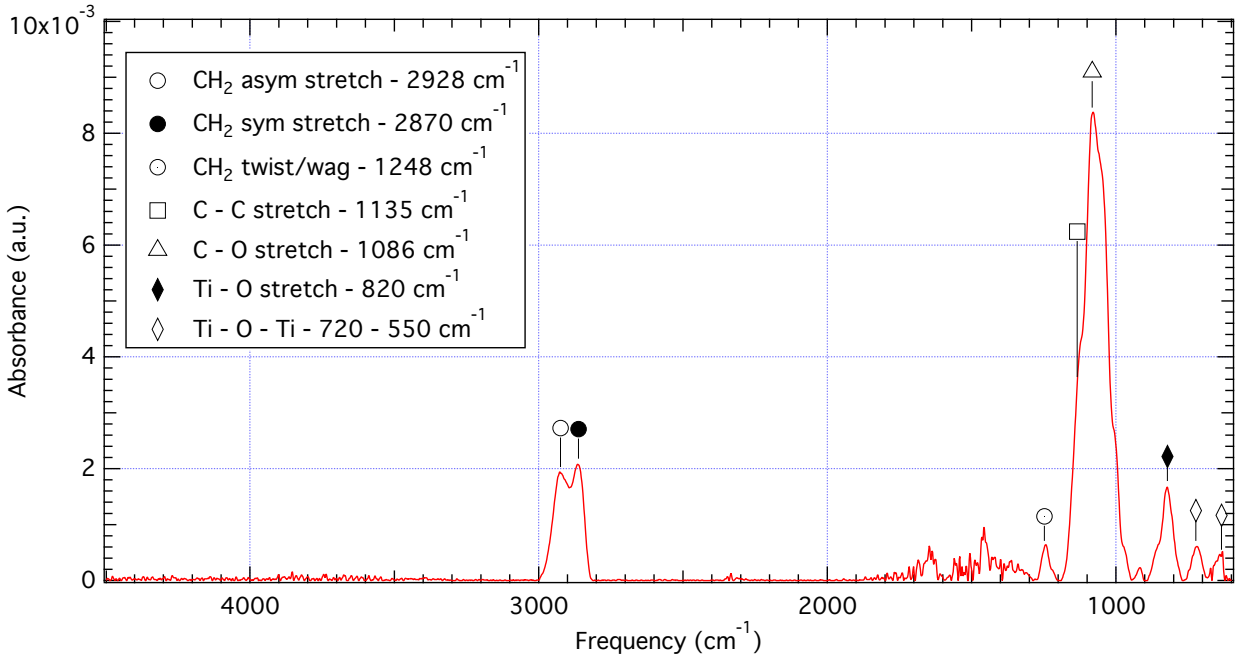

Figure 4: Infrared spectrum of an as-deposited titanicone film of 38 nm, deposited at 100 °C

Dalton Transactions Accepted Manuscript

wavenumbers, vibration modes related to the Ti-O bonds can be observed. More specifically, at 820 cm^{-1} a sharp peak assigned to the Ti-O stretch mode is present. In the range 720 to 550 cm^{-1}, a band of absorptions related to Ti-O-Ti bonds can be seen[26]. The combination of both the carbon related groups and the Ti absorptions provide evidence for the successful deposition of a hybrid organic-inorganic film containing titanium. In order to quantify the amount of carbon incorporated into the film, XPS measurements were performed. The expected elements (Ti, O and C) appear in the spectrum. The carbon peak remains after several sputtering steps, thus proving that the carbon is effectively incorporated into the film. For calculation of the atomic concentration of the elements, the Ti_{2p}, O_{1s} and C_{1s} regions were scanned in more detail, resulting in the following estimates: 25.8% titanium, 53.4% oxygen and 20.8% carbon. It can be noted that the ratio of titanium to oxygen is approximately the same as for regular TiO_2. XRD measurements showed that the as-deposited film was amorphous as no diffraction peaks were observed.

SEM imaging and AFM were used to study the surface morphology of the film. From the AFM measurement, which is shown as an insert in figure 5, it is clear that the as-deposited surface is very smooth. The rms roughness from this image was calculated to be 0.35 nm. The SEM image displayed no visible features and confirms the film smoothness.

For the in situ monitoring of the MLD process, an optical model for the titanicone film had to be developed. An empirical Cauchy dispersion relation of the type $n(\lambda) = A + B/\lambda^2 + C/\lambda^4$ was chosen. The A,B and C parameters of this model were then calibrated by fitting the measured data to several samples for which the thickness was measured by XRR. This analysis yielded the following values for the parameters: A = 1.679, B = 7.30×10^3 nm^2 and C = 2.08×10^9 nm^4. The resulting model was very accurate for the deposited films and able to calculate the correct thickness by data fitting with a low mean squared error. In this model, the refractive index is 1.72 at a wavelength of 600 nm.

XRR measurements were performed for both the thickness calibration of the ellipsometry model, and the calculation of the film density through data fitting. The result of this analysis is presented in figure 5. The estimated film density is 2.2 g/cm^3. After deposition, several deposited films

Dalton Transactions Accepted Manuscript

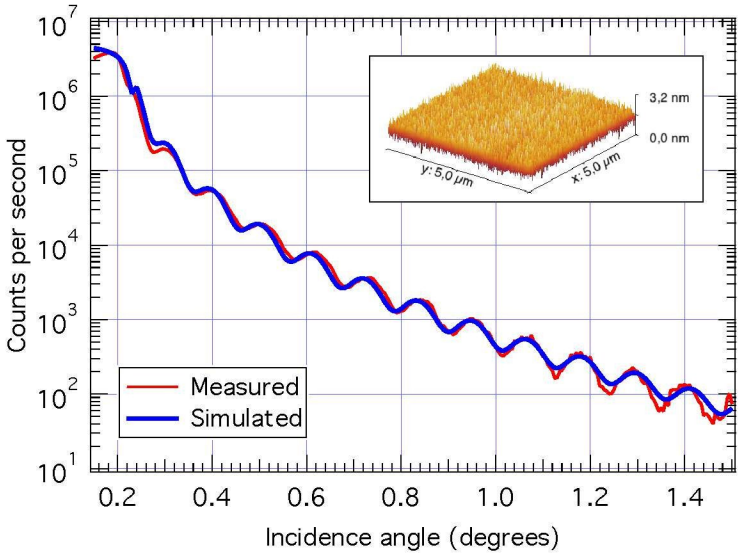

Figure 5: XRR measurement and simulation of a 38nm titanicone film for density calculation. An AFM measurement of the sample surface is presented as an insert.

were left exposed to ambient air for two weeks. Then, the XRR measurements were redone. No significant change in either the thickness or density of the films was observed. From this we can conclude that the films are stable in ambient air.

Water and heat treatment of titanicone films

A series of titanicone films, deposited with the same process parameters, was subjected to water and heat treatments. A total of 300 TDMAT/GL cycles were executed at a sample temperature of 100 °C. This corresponds to a starting film thickness of 24.6 nm. The titanicone films were deposited on Si substrates with either 100 nm thermal oxide, or an 80 nm Pt on 60 nm TiN stack. The last substrate was used only for the electrochemical measurements.

The water etching treatment consisted of submerging the as-deposited sample in deionized water for 5 days at room temperature. After approximately a few hours, bubbles started to form on the sample which is an indication of the removal of carbon groups from the hybrid layer, a phenomenon also reported for alucones[18]. Two separate heat treatments were also performed on as-deposited samples: annealing in air and helium atmospheres. During annealing, the temperature was ramped up at a rate of 10 °C/min to 500 °C. This temperature was held for 10 minutes before the heating

Dalton Transactions Accepted Manuscript

Table 2: Results of the EP measurements and analysis on the treated films.

	Porosity	Refr. index	Thickness (nm) [decrease]	Density (g/cm^3)
N	0%	1.72	24.6 [/]	2.2
W	21%	1.52	19.1 [22%]	1.9
A	2%	2.07	10.5 [57%]	4.3
H	1%	2.25	16.8 [32%]	3.1

was turned off and the samples cooled down back to room temperature. From this point the different samples will be referred to as follows: N for non-treated, A for annealed in air, H for annealed in helium and W for water etched.

In situ XRD was performed during the annealing experiments to monitor the possible formation of crystalline phases. The result of the XRD measurements for sample A is shown in figure 6. During annealing, sample A crystallized to the anatase TiO_2 phase. Almost all carbon was removed during annealing (as shown in XPS measurements later), which allowed the remaining TiO_2-like film to crystallize. The other sample types H and W remained amorphous after treatment.

EP measurements were performed on all samples to gauge possible porosity induced by the treatments. A summary of the results is presented in table 2. Only sample W showed a clear porosity of about 21% in the EP measurements. From the shape of the isotherms we can conclude that the

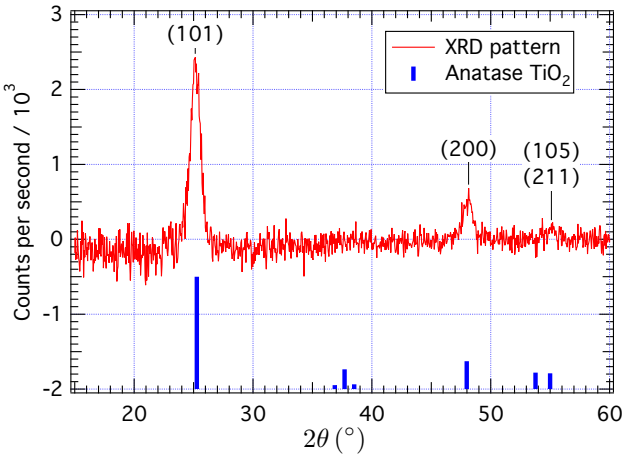

Figure 6: Ex situ XRD scan showing the crystallization to anatase TiO_2 after annealing in air at 500 °C.

Dalton Transactions Accepted Manuscript

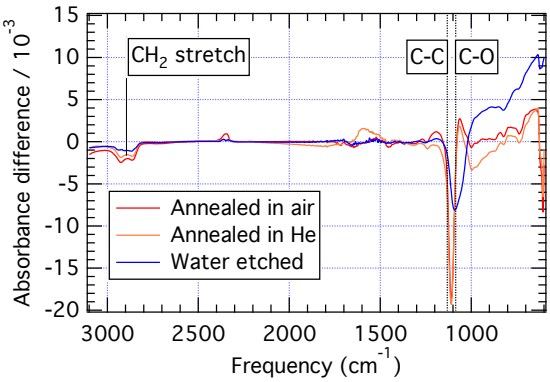

Figure 7: Absorbance difference in infrared spectroscopy of the treated samples, compared with the N sample.

pore shape is cylindrical. Performing extra analysis using the Brunauer-Emmett-Teller (BET) theory provides extra information on the pore size distribution (PSD). For sample W the PSD reached a maximum around the value of 1 nm.

The change in composition of the samples after the treatment was investigated using infrared spectroscopy (FTIR) and XPS. The result of the IR spectroscopy study is shown in figure 7. Here, the spectra presented are referenced to the N sample. Hence, the removal of chemical bonds from the film is indicated by negative peaks in the difference spectra. Focussing on the CH_2 stretch vibration modes, it is clear that a certain amount of these groups were removed by the different treatments. The removed fraction is smaller for the W sample than for the A and H samples. Looking at the C-C and C-O modes, there also appears to be a significant difference between the W and A/H samples. The position of the peaks shows that the water treatment impacts mainly the C-O bonds while the heat treatments focus on both C-C and C-O groups. The results from the XPS analysis are presented in table 3. It confirms the trend seen in infrared spectroscopy of the CH_2 vibration modes. For sample W a fraction of the total carbon content is removed, while for sample A no carbon remains after the calcination treatment. Sample H is however different. From XPS it is clear that all carbon is retained in the film although C-H, C-C and C-O bonds disappear as seen in infrared spectroscopy. From this we conclude that the carbon remains inside the H films in a different form which is not immediately evident.

Dalton Transactions Accepted Manuscript

Table 3: Comparison of the composition of the titanicone films in atomic concentrations, determined by XPS.

	C (%)	Ti (%)	O (%)
N	21	26	53
W	7	29	64
A	1	31	68
H	24	24	52

Electrochemical measurements on titanicone films

Both the non-treated and treated titanicone samples were tested as electrodes in a lithium-ion cell. For comparison purposes, two TiO_2 reference films were deposited by 300 cycles TDMAT/H_2O thermal ALD. This resulted in a thickness of 11 nm. One film was kept amorphous while the other received an identical annealing treatment to sample A. XRF was employed to compare the amount of titanium in the reference samples to the titanicone films. The integrated area below the Ti XRF peak is proportional to the amount of Ti atoms in the film. The electrochemical data for the reference samples shown here was normalized to the same amount of Ti as in the titanicone films, to make the comparison more straightforward.

First, the potential was swept in a potential range of 0.8 to 3.2V versus Li^+/Li during cyclic voltammetry. The resulting cyclic voltammograms are shown in figure 8. Sample N displayed no oxidation or reduction peaks during cycling, so we conclude that the as-deposited film is electrochemically inactive towards lithium ion insertion in this potential range. The treated samples did show charging and discharging behavior during CV measurements. For all samples, except for W, the CV stabilizes after 5 lithium insertion and extraction cycles. Sample A showed a clear reduction and oxidation (Li^+ insertion and extraction) peak centered around 1.91 V vs Li^+/Li. This is very close to the average peak position at 1.96 V vs Li^+/Li for the anatase reference. The shape of the voltammograms also was very similar. Both in the voltammograms for sample H and the amorphous reference very broad current waves were observed. For the amorphous reference, the average peak position was 1.17 V vs Li^+/Li. No clear peaks could be discerned in the voltammo-

Dalton Transactions Accepted Manuscript

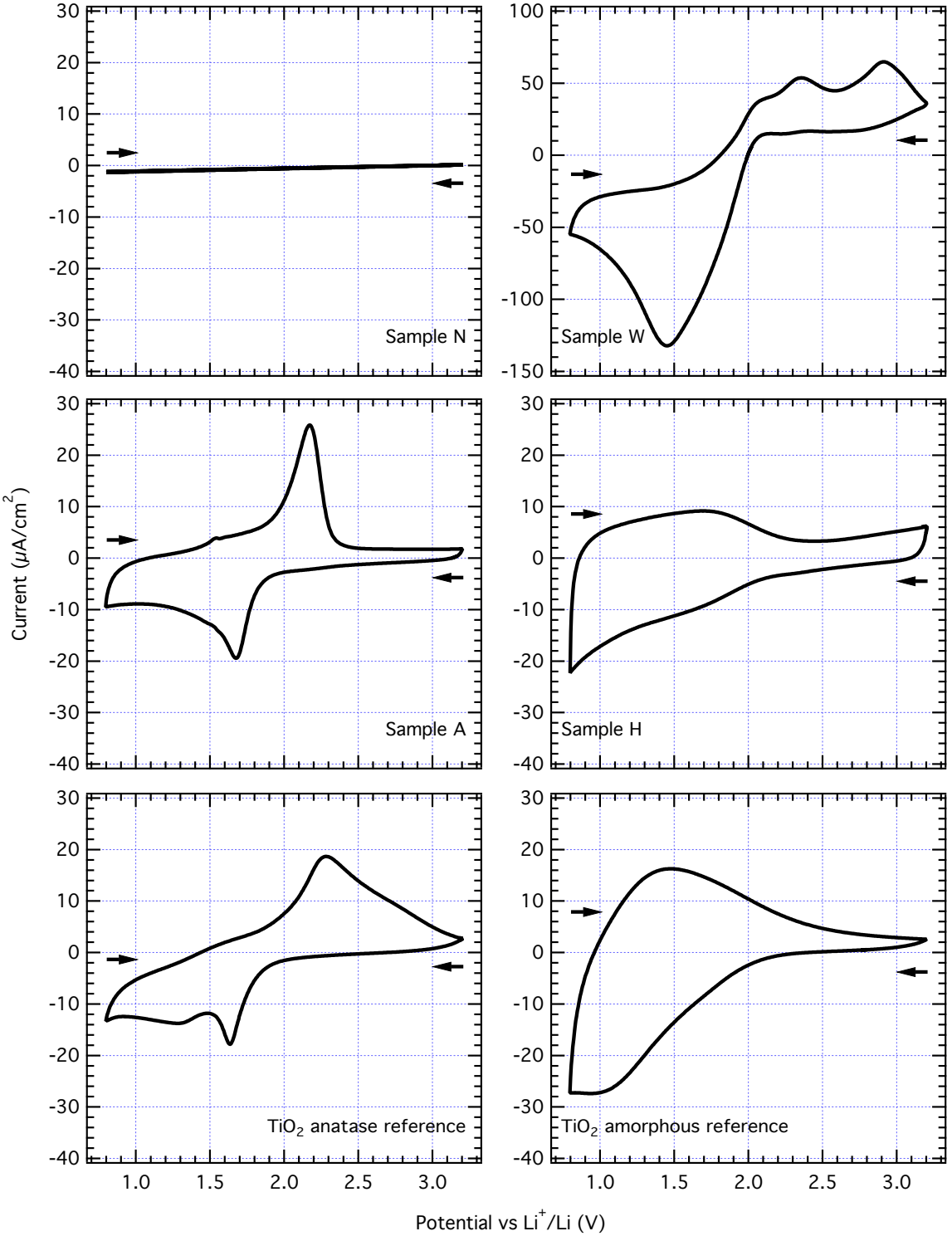

Figure 8: Cyclic voltammograms of all samples, taken at a scan rate of 10 mV/s in the potential range of 0.8 to 3.2 V versus Li^+/Li. The arrows indicate the scan direction. The 5th scan after initial stabilization is shown, except for sample W where the 15th scan is displayed.

Dalton Transactions Accepted Manuscript

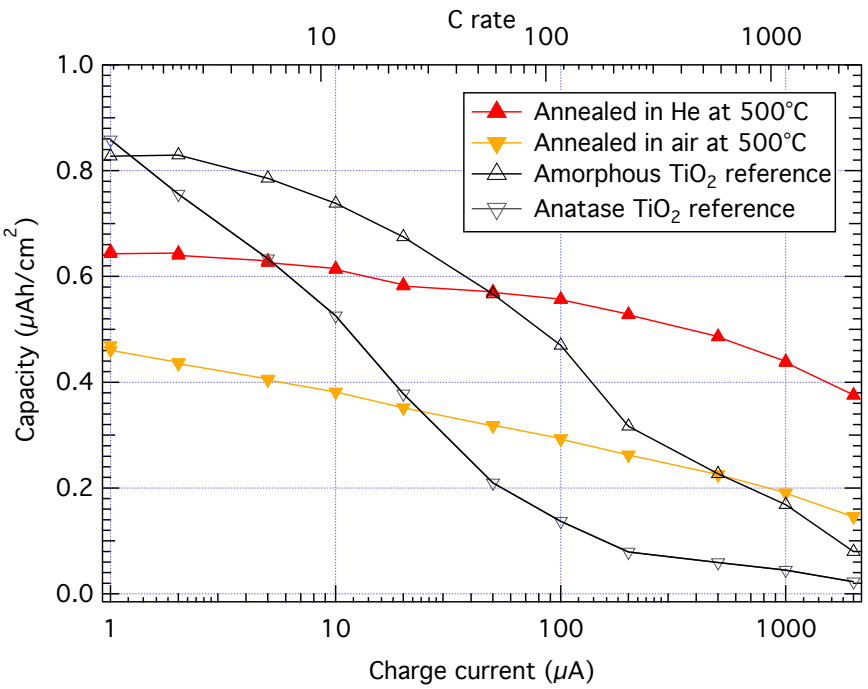

Figure 9: Comparison of the delithiation capacity densities of the treated and reference samples with increasing charge/discharge current

gram of sample H, hence no average position is reported. The similar shape of the voltammograms is consistent with the amorphous nature of sample H measured with XRD. Sample W showed drastically different behavior than the other samples. During cycling, the reduction and oxidation peaks kept increasing until the CV stabilized after 15 cycles. A large reduction peak was found at 1.45 V vs Li^+/Li. Two oxidation peaks appeared at 2.36 and 2.90 V vs Li^+/Li. The voltammogram did not exhibit typical capacitive behavior since the sign of the current remained unchanged after switching the scan direction. Instead, two current plateaus were observed which are indicative of homogeneous reactions occurring at the electrode. Cyclic voltammetry measurements on a bare Pt sample revealed an almost identical behavior. It appears that the electrolyte is in direct contact with the current collector and was therefore capable of reacting chemically with Pt during the CV measurements. This observation is complementary to the porous nature of the water etched samples seen during EP measurements.

After the cyclic voltammetry measurements, charging and discharging experiments were performed on the same samples. The charging and discharging current was increased stepwise for

Dalton Transactions Accepted Manuscript

each charge and discharge cycle, starting at 1 µA and ending at 10 mA. Every time the current had reached an order of magnitude increase, the next cycle was performed at the starting current of 1 µA. This way the stability of the electrodes could be checked and possible degradation would be noticed. For all samples, except N and W, there was no noticeable decrease in delithiation capacity in this experiment. Samples N and W were excluded from these measurements because they showed respectively no activity or no capacitive behavior during cyclic voltammetry.

The delithiation capacity is presented as a function of charge current in figure 9. At low charge currents, the reference samples showed a larger capacity than any of the titanicone samples. However, at increasing currents the capacity of the reference samples dropped faster than the heat treated samples. Sample H showed the most promising results. For charge currents above 5 µA, it performed better than the anatase reference. Above 50 µA, it even improved on the amorphous reference sample. At a charge current of 2 mA the delithiation capacity of the He annealed sample was 4.7 times higher than the capacity of the amorphous reference sample. This improved rate performance can most likely be attributed to an increased conductivity caused by the carbon inside the film[19]. Sample A also displayed improved capacity at higher currents, although the difference with the references was less pronounced as with sample H. At currents above 20 µA, the capacity rose above the value for the anatase reference. Beyond 500 µA there was a slight gain over the amorphous reference.

Conclusions

In this work, two novel processes for the molecular layer deposition of titanicone were investigated, using TDMAT as the titanium precursor. For the TDMAT/EG process, growth is quickly terminated after about 10 cycles, presumably caused by double surface reactions of the EG. The TDMAT/GL process on the other hand shows typical MLD behavior with good linearity versus cycle number and a saturated growth rate at long enough TDMAT and GL pulse times. The temperature window for the process ranges from 80 °C to 160 °C with the respective growth rates

Dalton Transactions Accepted Manuscript

decreasing from 0.95 Å/cycle to 0.24 Å/cycle. The hybrid nature of the as-deposited films was confirmed with both FTIR and XPS, showing a carbon content of about 20%. From AFM and SEM measurements, it was clear that the films were smooth, having a low rms surface roughness of 0.35 nm. The density of the film was estimated at 2.2 g/cm^3 and the refractive index was 1.72 at a wavelength of 600 nm.

Three different post-deposition treatments were performed on the as-deposited films: annealing up to 500 °C in inert (He) and oxidizing (air) atmospheres, and water etching. For both the air annealed and water etched samples, carbon was removed from the film. However, for the He annealed samples the carbon content remained unaltered. After the treatments, EP revealed about 20% porosity in the water etched sample and none in the other samples. The air annealed sample was transformed to anatase TiO_2. All treated samples were electrochemically active, as opposed to the as-deposited films. The water etched samples showed no capacitive behavior during cyclic voltammetry because the porous nature of the film allowed direct contact between the electrolyte and the Pt current collector. Both the air and He annealed samples displayed an improved rate performance when compared to their respective anatase and amorphous TiO_2 references. The He annealed samples showed the highest capacity of all treated samples. At a charge current of 2 mA, its capacity was 4.7 times higher than the capacity of the amorphous reference. This result may open up a possible application for this film as buffer layer to improve the rate performance of an existing bulk electrode material.

Acknowledgement

The authors are grateful to the FWO Vlaanderen for providing Kevin Van de Kerckhove with financial support through the mandate of Aspirant, and for financial support from the IWT-SBO SOSLion project. They also thank ir. Kilian Devloo-Casier and Matthias Minjauw for the XPS measurements, and Olivier Janssens for SEM/EDX work.

Dalton Transactions Accepted Manuscript

References

(1) George, S. M. *Chemical Reviews* **2010**, *110*, 111–131.

(2) Yoshimura, T.; Tatsuura, S.; Sotoyama, W. *Applied Physics Letters* **1991**, *59*, 482–484.

(3) Bertrand, J. A.; Dameron, A. A.; Seghete, D.; Burton, B. B.; Davidson, S. D.; Cavanagh, A. S.; George, S. M. *Chemistry of Materials* **2008**, *20*, 3315–3326.

(4) Lee, B. H.; Yoon, B.; Anderson, V. R.; George, S. M. *The Journal of Physical Chemistry C* **2012**, *116*, 3250–3257.

(5) Park, Y.; Han, K. S.; Lee, B. H.; Cho, S.; Lee, K. H.; Im, S.; Sung, M. M. *Organic Electronics* **2011**, *12*, 348–352.

(6) Chen, C.; Li, P.; Wang, G.; Yu, Y.; Duan, F.; Chen, C.; Song, W.; Qin, Y.; Knez, M. *Angewandte Chemie International Edition* **2013**, *52*, 9196–9200.

(7) Yoon, B.; Seghete, D.; Cavanagh, A. S.; George, S. M. *Chemistry of Materials* **2009**, *21*, 5365–5374.

(8) Lee, Y.; Yoon, B.; Cavanagh, A. S.; George, S. M. *Langmuir* **2011**, *27*, 15155–15164.

(9) Klepper, K. B.; Nilsen, O.; Hansen, P.-A.; Fjellvåg, H. *Dalton Transactions* **2011**, *40*, 4636.

(10) Yoon, B.; O'Patchen, J. L.; Seghete, D.; Cavanagh, A. S.; George, S. M. *Chemical Vapor Deposition* **2009**, *15*, 112–121.

(11) Peng, Q.; Gong, B.; VanGundy, R. M.; Parsons, G. N. *Chemistry of Materials* **2009**, *21*, 820–830.

(12) Lee, B. H.; Anderson, V. R.; George, S. M. *Chemical Vapor Deposition* **2013**, *19*, 204–212.

(13) Lee, B. H.; Anderson, V. R.; George, S. M. *ACS Applied Materials & Interfaces* **2014**, *6*, 16880–16887.

Dalton Transactions Accepted Manuscript

(14) Nilsen, O.; Klepper, K.; Nielsen, H.; Fjellvåg, H. *ECS Transactions* **2008**, *16*, 3–14.

(15) Abdulagatov, A. I.; Hall, R. A.; Sutherland, J. L.; Lee, B. H.; Cavanagh, A. S.; George, S. M. *Chemistry of Materials* **2012**, *24*, 2854–2863.

(16) Sundberg, P.; Karppinen, M. *European Journal of Inorganic Chemistry* **2014**, *2014*, 968–974.

(17) Sood, A.; Sundberg, P.; Malm, J.; Karppinen, M. *Applied Surface Science* **2011**, *257*, 6435–6439.

(18) Liang, X.; Yu, M.; Li, J.; Jiang, Y.-B.; Weimer, A. W. *Chemical Communications* **2009**, 7140–7142.

(19) Abdulagatov, A. I.; Terauds, K. E.; Travis, J. J.; Cavanagh, A. S.; Raj, R.; George, S. M. *Journal of Physical Chemistry C* **2013**, *117*, 17442–17450.

(20) Moitzheim, S.; Nimisha, C. S.; Deng, S.; Cott, D. J.; Detavernier, C.; Vereecken, P. M. *Nanotechnology* **2014**, *25*, 504008.

(21) Xie, Q.; Jiang, Y.-L.; Detavernier, C.; Deduytsche, D.; Van Meirhaeghe, R. L.; Ru, G.-P.; Li, B.-Z.; Qu, X.-P. *Journal of Applied Physics* **2007**, *102*, 083521.

(22) Xie, Q.; Musschoot, J.; Deduytsche, D.; Van Meirhaeghe, R. L.; Detavernier, C.; Van den Berghe, S.; Jiang, Y.-L.; Ru, G.-P.; Li, B.-Z.; Qu, X.-P. *Journal of the Electrochemical Society* **2008**, *155*, H688–H692.

(23) Longrie, D.; Deduytsche, D.; Haemers, J.; Smet, P. F.; Driesen, K.; Detavernier, C. *ACS Applied Materials & Interfaces* **2014**, *6*, 7316–7324.

(24) Baklanov, M. R.; Mogilnikov, K. P.; Polovinkin, V. G.; Dultsev, F. N. *Journal of Vacuum Science & Technology B* **2000**, *18*, 1385–1391.

(25) Dendooven, J.; Devloo-Casier, K.; Levrau, E.; Van Hove, R.; Sree, S. P.; Baklanov, M. R.; Martens, J. A.; Detavernier, C. *Langmuir* **2012**, *28*, 3852–3859.

Dalton Transactions Accepted Manuscript

(26) Vasconcelos, D.; Costa, V. C.; Nunes, E. H. M.; Nunes, E.; Sabioni, A. C. S.; Gasparon, M.; Vasconcelos, W. L. *Materials Sciences and Applications* **2011**, *2*, 1375–1382.

Dalton Transactions Accepted Manuscript

Post-deposition heat and water treatments activate MLD titanicone as a lithium-ion battery anode

Dalton Transactions Accepted Manuscript

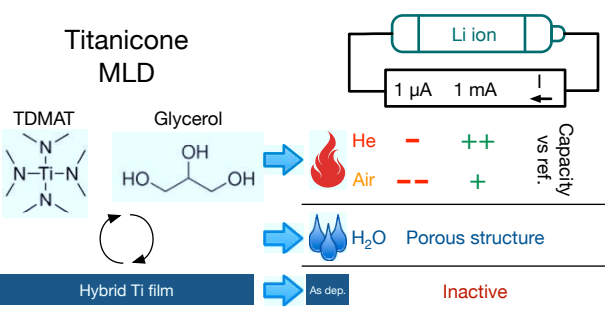

Dalton Transactions Accepted Manuscript